Reliable Frequency-Hopping MIMO Radar-based Communications with Multi-Antenna Receiver

Kai Wu, J. Andrew Zhang, *Senior Member, IEEE*, Xiaojing Huang, *Senior Member, IEEE*, Y. Jay Guo, *Fellow, IEEE*, and Jinhong Yuan, *Fellow, IEEE*

***Abstract*—Frequency-hopping (FH) MIMO radar is recently introduced as an underlying system for realizing dual-function radar-communication (DFRC), increasing communication symbol rates to multiples of the radar pulse repetition frequency. As a newly conceived DFRC system, many realistic issues, such as channel estimation and synchronization, are not effectively solved yet. In this paper, we develop a multi-antenna receiver-based downlink communication scheme for the FH-MIMO DFRC, addressing the above issues in multi-path channels. By exploring the unique FH-MIMO radar waveform, we suppress both inter-antenna and inter-hop interference, and introduce minimal constraints on the radar waveform to facilitate DFRC. We then develop accurate estimation methods for timing offset and channel parameters. These methods are further employed to design reliable demodulation methods. We also derive performance bounds for the proposed estimation methods and embedded communications. Simulation results validate the efficacy of our receiving scheme, showing that the performance of estimators and data communications approaches analytical bounds.**

***Index Terms*—Joint communication and radar/radio sensing (JCAS), dual-function radar-communication (DFRC), frequency hopping (FH), MIMO, timing offset, channel estimation, maximum ratio combining (MRC) and antenna diversity.**

I. Introduction

The convergence of wireless communications and radar sensing becomes increasingly promising and has been envisioned as a key feature of future 6G networks [1]. Integrating the two functions into one by sharing hardware and signal processing modules achieves immediate benefits of reduced cost, size, weight, and better spectrum efficiency [2]. It can further help each other to improve the performance and capability of the communication and sensing. The design of joint radar and communication systems can be communication-centric and radar-centric [3]. The former performs radar sensing using ubiquitous communication signals, e.g., IEEE 802.11p [4] and IEEE 802.11ad [5]–[7], whereas the later embeds information bits into existing radar waveform, e.g., frequency modulated continuous wave [8] and linear frequency modulation wave [9], or jointly optimized waveform, particularly in MIMO radars [10], [11].

Manuscript received XXX, XX, 2020. This work is partially funded by the NSW Defence Innovation Network and the NSW State Government through Pilot Project grant DINPP-19-20 10.01

K. Wu, J. A. Zhang, X. Huang and Y. J. Guo are with the Global Big Data Technologies Centre, University of Technology Sydney, Sydney, NSW 2007, Australia (e-mail: kai.wu@uts.edu.au; andrew.zhang@uts.edu.au; xiaojing.huang@uts.edu.au; jay.guo@uts.edu.au).

J. Yuan is with the University of New South Wales, Sydney, NSW 2052, Australia (e-mail: j.yuan@unsw.edu.au).

As a complement to the communication-centric counterpart, radar-centric designs, also referred to as dual-function radar-communication (DFRC), can be more competent in achieving long-distance (tens to hundreds of kilometers) data communication between a radar and an aircraft [12]. Many existing DFRC designs embed information symbol on a basis of one or multiple radar pulses, and hence their communication symbol rate is limited to radar pulse repetition frequency (PRF) [13]. In some recent works [14]–[22], frequency-hopping MIMO (FH-MIMO) radars are introduced to DFRC, which substantially increases the symbol rate to multiples of (e.g., 15 times) PRF. The benefit is obtained from the unique FH-MIMO waveform dividing each radar pulse into multiple sub-pulses (also referred to as hops) [23].

There are two types of information modulation in FH-MIMO radar-based DFRC (FH-MIMO DFRC), one based on conventional phase modulation [14]–[16] and the other exploiting the diversity of hopping frequencies [18], [21]. In [14], [15], phase shift keying (PSK) modulations are introduced to FH-MIMO DFRC by embedding PSK phases to radar signals. To reduce out-of-band transmissions and range sidelobe levels of radar, differential PSK (DPSK) [16] and continuous phase modulation (CPM) [17] are exploited in FH-MIMO DFRC. In [18], combinations of hopping frequencies are used to convey information bits, referred to as frequency hopping code selection (FHCS). To improve data rate, PSK and FHCS are jointly used in [19], [20]. In [21], permutations of hopping frequencies are further exploited for achieving secure FH-MIMO DFRC. In [22], the above schemes [14]–[18] are also compared with respect to (w.r.t.) their impact on radar ranging. In [12], comprehensive comparisons among the above schemes are provided w.r.t. both radar and communication performance.

To detect the transmitted information at the user end (UE), the channel information is required for most phase modulation schemes [14], [15], [17], [19], [20], and accurate timing is essential to all the above-mentioned designs [14]–[22] to avoid inter-antenna and inter-hop interference. In most previous works, perfect channel information and timing are assumed. However, their estimations are challenging in FH-MIMO DFRC for the following main reasons. *First*, unlike in conventional communication systems, there is a lack of specific signaling for synchronization or channel estimation here. *Second*, due to the lack of a specific synchronization link, there can be a non-negligible timing offset, which leads to inter-hop and inter-antenna interference [20], as will be detailed in Section II-B. *Third*, the phase disturbances caused by a non-negligible timing offset and channel responses are

coupled in a point-wise multiplicative manner, making the overall channel change rapidly over hops (time). This will be illustrated in Section III. Another presumption in most DFRC designs [14]–[18] is that the UE knows the hopping frequency used by each transmitter antenna of the FH-MIMO radar at any hop. This can be non-trivial to realize, considering that the radar can change hopping frequencies frequently, e.g., on the basis of radar pulse, for the reasons like avoiding co-channel interference/jamming.

Thus far, only a few works [19], [20], [24], [25] have developed channel estimation methods for radar-based DFRC systems. In [24], [25], sparse recovery-based channel estimation methods are developed, which coordinate radar and communication receiver using probing beams. In [19], a novel FH-MIMO radar waveform is designed, enabling a UE to estimate the hopping frequencies used by the radar at any hop; accordingly, an accurate channel estimation method is designed for line-of-sight (LoS) scenarios. However, the work in [19] is based on perfect timing. In [20], the timing offset estimation is investigated for FH-MIMO DFRC systems with two high-accuracy estimators developed for hopping frequency sequences with different features. The work, however, is mainly based on an LoS channel and a single-antenna UE receiver. Although extensions to multi-path and multi-antenna cases are discussed therein, the benefit of introducing multiple antennas at a UE, e.g., using antenna diversity to combat multi-path fading, has not been explored yet. In a different yet relevant context (spectrum sharing), interference channel between radar and communication is estimated to achieve co-existence [26]–[28]. In some recent DFRC works [2], [29], channel estimation methods are developed for new (future) DFRC waveforms/platforms. These methods [2], [26]–[29] are not directly applicable to FH-MIMO DFRC; refer to [20, Section I-B] for an overview.

To achieve reliable FH-MIMO DFRC, we develop in this paper a multi-antenna receiving scheme for the challenging yet practical FH-MIMO DFRC scenarios — the radar performs downlink communication with a UE through multi-path channels, while randomly changing hopping frequencies for sensing without alerting the UE. Specifically, we propose new estimation methods for channel parameters and timing offset, as well as the multi-antenna information demodulation approach. The key contributions are summarized as follows.

1) We explore the unique FH-MIMO radar waveform and devise a special discrete time-frequency transformation, which leads to a clear signal structure in FH-MIMO DFRC. We discover that under certain conditions regarding the radar parameters, the above transformation can eliminate the inter-hop and inter-antenna interference, even in the presence of timing offset;
2) We exploit the degrees of freedom embedded in the radar waveform and develop accurate estimation methods for both timing offset and channel responses. In particular, we propose a way of assigning the zero-th sub-band for certain antennas and hops, which eliminates the impact of timing offset on the estimation of channel responses;
3) We also formulate the estimation of timing offset into the problem of estimating the frequency of a single-tone signal. A low-complexity and high-accuracy estimator is provided for estimating the timing offset. Based on the value of timing offset, there can be an estimation ambiguity. An effective solution is also developed to eliminate the ambiguity;
4) We derive the analytical mean squared error (MSE) of the achieved channel estimation, and the Cramér-Rao lower bound (CRLB) for the timing offset estimation. We also analyze the achievable rate and symbol error rate (SER) of the FH-MIMO DFRC performing the proposed multi-antenna receiving scheme;
5) Extensive simulations validate the high accuracy of the proposed estimation methods and the superior communication reliability achieved by the proposed receiving scheme. Notably, the SER of FH-MIMO DFRC is improved by orders of magnitude when the number of antennas at the UE increases from one to two, which highlights the significance of the proposed multi-antenna receiving scheme.

With the new designs summarized above, we underline below the main reasons why the proposed scheme can greatly enhance the reliability of FH-MIMO DFRC. *First*, a multi-antenna receiver is equipped at UE, which allows the antenna diversity to be exploited for both the detection of hopping frequencies and the demodulation of the PSK symbols. This will be detailed in Section IV-C. *Second*, the timing offset is accurately estimated and compensated, so that the accurate detection of hopping frequencies can be achieved at the UE. *Third*, the channel responses between each pair of transmitter and receiver antennas are accurately estimated, which enables us to perform the maximum-likelihood combining (MRC) at the UE to achieve the maximal improvement on the signal-to-noise ratio (SNR) when demodulating PSK symbols.

The remainder of the paper is organized as follows. The signal model of FH-MIMO DFRC is described in Section II. Then the DFRC signal model is simplified in Section III, drawing some useful insights. The proposed multi-antenna receiving scheme is presented in Section IV, where the estimation methods for channel parameters and timing offset, as well as the information demodulation are developed in sequence. Performance analysis is provided in Section V, followed by simulations in Section VI. Section VII concludes the paper and provides future works.

Notations: Bold upper- and lower-case letters denote matrices and vectors, respectively. $\mathbb{I}_+$ denotes the set of positive integers. $|\cdot|$ can take amplitude, absolute and cardinality, depending on context. $(\cdot)^{\mathrm{T}}$ takes transpose. $\lfloor\cdot\rceil$, $\lfloor\cdot\rfloor$ and $\lceil\cdot\rceil$ rounds towards nearest integer, the negative infinity and the positive infinity, respectively. C_M^K denotes binomial coefficient. $\delta(l)$ denotes the discrete Dirac delta function. $[\mathbf{x}]_n$ takes entry n of a vector $\mathbf{x}$. Variables with subscripts $()_h$ and $()_m$ indicate their associations with hop h and antenna m, respectively. In general, $\hat{x}$ (with a hat accent) denotes an estimate, and $\underline{\mathsf{P}}$ (with an underline) denotes a lower bound.

II. Signal Model

An FH-MIMO DFRC system is illustrated in Fig. 1(a), where an FH-MIMO radar senses a target while communicat-

ing with a UE through flat-fading multi-path channels. Both the radar and UE are equipped with a uniform linear array whose antenna spacing is half a wavelength. In this section, we provide the signal models of the radar and DFRC.

A. Signal Model of FH-MIMO Radar

The FH-MIMO radar is based on fast frequency hopping. Each pulse is divided into H sub-pulses, also referred to as *hops* [18]. The centroid frequency of the transmitted signal changes randomly across hops and antennas, as illustrated in Fig. 1(b). Denote the radar bandwidth as B. By dividing the frequency band evenly into K sub-bands, the baseband frequency of the k-th sub-band is given by $f_k = \frac{kB}{K}$ $(k = 0, 1, \cdots, K-1)$. Let M denote the number of antennas in the radar transmitter array[1]. We have $M < K$ in FH-MIMO radar. Out of the K centroid frequencies, M frequencies are selected to be the hopping frequencies at a hop, one per antenna. Denote the hopping frequency at hop h and antenna m as f_{hm}, then

$$f_{hm} = k_{hm}B/K,\ k_{hm} \in \{0, 1, \cdots, K-1\}. \tag{1}$$

To ensure the orthogonality between the waveforms from the different antennas of FH-MIMO radar, the following are required on radar parameters [23]

$$k_{hm} \neq k_{hm'}\ (\forall m \neq m',\ \forall h);\ \Delta \triangleq BT/K \in \mathbb{I}_+, \tag{2}$$

where T is hop duration, and the shorthand symbol Δ is introduced for notational simplicity. At hop h the m-th antenna of the radar transmitter sends

$$s_{hm}(t) = e^{\mathrm{j}2\pi f_{hm}t} g_{\mathrm{rect}}(t - hT),\ 0 \leq t \leq T. \tag{3}$$

Here, $g_{\mathrm{rect}}(t)$ denotes the rectangular function taking unit one if $0 \leq t \leq T$ and otherwise zero. Refer to [20, Appendix X-A] for an elaboration on FH-MIMO radar signal processing.

B. DFRC Signal Model

Consider P paths between the radar and UE, each having the AoD of ϕ_p, the AoA of θ_p and the complex path gain of β_p. Assuming quasi-static channels in a short radar pulse, it follows that ϕ_p, θ_p and β_p are independent of h [31]. The steering vectors of radar and UE arrays are $\mathbf{a}_M(u_p)$ and $\mathbf{a}_N(\nu_p)$, respectively. They are given by

$$\begin{aligned} \mathbf{a}_M(u_p) &= [1, e^{\mathrm{j}u_p}, \cdots, e^{\mathrm{j}(M-1)u_p}]^{\mathrm{T}},\ u_p = \pi \sin\phi_p; \\ \mathbf{a}_N(\nu_p) &= [1, e^{\mathrm{j}\nu_p}, \cdots, e^{\mathrm{j}(N-1)\nu_p}]^{\mathrm{T}},\ \nu_p = \pi \sin\theta_p, \end{aligned} \tag{4}$$

where N is the number of antennas in the UE array. To perform data communication, a PSK modulation signal[2], as given by

$$F_{hm} = e^{\mathrm{j}\varpi_{hm}},\ \varpi_{hm} \in \Omega_{J_{\mathrm{PSK}}}\ (J_{\mathrm{PSK}} \geq 1), \tag{5}$$

can be multiplied with $s_{hm}(t)$ to embed information bits in radar signal [14], where $\Omega_{J_{\mathrm{PSK}}} = \left\{0, \cdots, \frac{2\pi(2^{J_{\mathrm{PSK}}}-1)}{2^{J_{\mathrm{PSK}}}}\right\}$ is the J_{PSK}-bit PSK constellation.

To fulfill data communications and reduce overhead, we consider packet communications and employ the signal frame structure as shown in Fig. 1(b). In each frame, the first radar hop is assigned for estimating timing offset and channel; and the remaining hops are used for data transmission. Unlike may existing works based on a perfect timing [22], we consider more practical scenarios that the UE performs a coarse timing based on the conventional energy-based or auto-correlation-based packet detection [28], resulting in a timing offset η. In general, $\eta < \frac{T}{2}$ can be ensured [32], which is assumed in the following. Let $f_{\mathrm{s}} (\geq 2B)$ denote the sampling frequency; the sampling interval is then $T_{\mathrm{s}} = 1/f_{\mathrm{s}}$. The number of samples in T and η are given by $L = \lfloor \frac{T}{T_{\mathrm{s}}} \rceil$ and $L_\eta = \lfloor \frac{\eta}{T_{\mathrm{s}}} \rceil$, respectively.

Based on (3) and (4), the UE-received baseband signal at hop h can be given by the following $N \times 1$ vector,

$$\mathbf{y}_h(i) = \sum_{p=0}^{P-1} \left(\beta_p \sum_{m=0}^{M-1} \tilde{s}_{hm}(i) e^{\mathrm{j}mu_p} \right) \mathbf{a}_N(\theta_p) + \mathbf{n}_h(i), \tag{6}$$

where i is the sample index and $\mathbf{n}_h(i) \in \mathbb{C}^{N\times 1}$ collects N independent and identically distributed (IID) AWGNs on the UE antennas. In (6), $\tilde{s}_{hm}(i)$ is the sampled signal of $F_{hm}s_{hm}(t)$ at hop h. Given $\eta > 0$, $\tilde{s}_{hm}(i)$ can span over two actual radar hops, as illustrated in Fig. 1(b). Taking the sampled hop 1 for an illustration, we see from Fig. 1(b) that the sampled hop consists of the actual hops 0 and 1. The interference caused by hop 0 to hop 1 is referred to as the *inter-hop interference*. Considering that the starting point of sampled hop h is earlier than the actual point, $\tilde{s}_{hm}(i)$ is given by

$$\begin{aligned} \tilde{s}_{hm}(i) &= \begin{cases} F_{(h-1)m}s_{(h-1)m}(i + L - L_\eta) & i \in \mathcal{I}_1 \\ F_{hm}s_{hm}(i - L_\eta) & i \in \mathcal{I}_2, \end{cases} \\ \text{s.t.}\ \ &\mathcal{I}_1 = \{0, 1, \cdots, L_\eta - 1\};\ \mathcal{I}_2 = \{L_\eta, \cdots, L-1\}. \end{aligned} \tag{7}$$

In (7), $s_{hm}(i)$ is the digitized $s_{hm}(t)$ given in (3), specifically

$$s_{hm}(i) = e^{\mathrm{j}\frac{2\pi k_{hm}B}{K} i T_{\mathrm{s}}} = e^{\mathrm{j}\frac{2\pi k_{hm}\Delta}{L} i}, \tag{8}$$

where Δ is defined in (2). Based on (7), we can validate that the inner product between $\tilde{s}_{hm}(i)$ and $\tilde{s}^*_{hm'}(i)$ $(\forall m' \neq m)$ is non-zero, i.e., $\sum_{i=0}^{L-1} \tilde{s}^*_{hm}(i)\tilde{s}_{hm'}(i) \neq 0$. To this end, the signal transmitted by antenna m causes interference to that by antenna m', or vice versa. This interference is referred to as the *inter-antenna interference* which prevents UE from extracting the signal component related to a single antenna (which is achievable without inter-antenna interference). Note that accurate signal extraction is critical to information demodulation, as will be seen in Section IV-C.

III. Investigating DFRC Signal Mode

In this section, we first simplify the DFRC signal model to disclose the hidden feature, and then draw some insights into the simplified signal model which will be useful in developing the proposed receiving scheme. From (6), we notice that the signals transmitted by all the radar transmitter antennas are

[1]Note that FH-MIMO radar is a type of orthogonal MIMO radar which generally has multiple antennas for both transmitter and receiver. One of the benefits of the multi-antenna configuration is to obtain an extended array aperture and hence a fine spatial resolution [30].

[2]For ease of exposition, we employ PSK [14] to develop the proposed receiving scheme, given the much simpler signal models than those of DPSK [16] and CPM [17]. Note that the proposed methods can be readily applied to other modulations exploiting the proposed methods, as will be developed in Section IV.

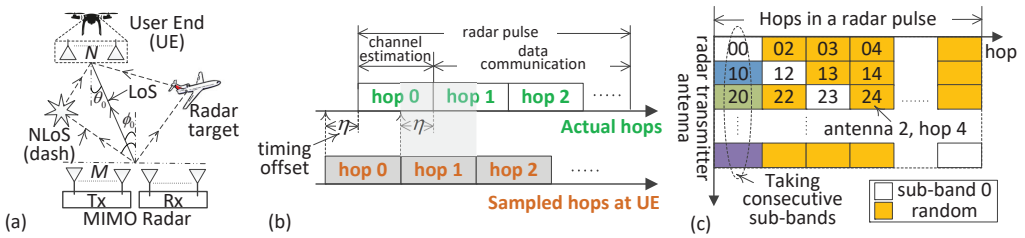

Fig. 1. (a) Illustration on the system diagram of an FH-MIMO DFRC; (b) the signal frame structure devised for the downlink communication, where the timing offset η is smaller than half the time duration of a hop; (c) illustration of the proposed arrangement of hopping frequencies over antennas and hops.

superimposed at the UE receiver. Provided a perfect timing, we can employ the waveform orthogonality, as given in (2), to separate the signals in the frequency domain [19]. However, in the presence of a non-zero timing offset η, as illustrated in Fig. 1(b), inter-hop interference is introduced and the waveform orthogonality is lost. We notice that the unique signal structure of the FH-MIMO radar can be exploited to combat the adverse consequence of η.

In particular, we propose to take the L-dimensional yet $\frac{L}{2}$-point DFT of $y_{hn}(i)$ $(i = L/2, \cdots, L-1)$ to avoid inter-hop interference, where $y_{hn}(i)$, $\forall i$, denotes the n-th entry of $\mathbf{y}_h(i)$, $\forall i$, as given in (6). This leads to

$$\begin{aligned} Y_{hn}(l) &= \frac{2}{L}\sum_{i=L/2}^{L-1} y_{hn}(i) e^{-\mathrm{j}\frac{2\pi i l}{L}} \\ &= \sum_{p=0}^{P-1}\beta_p \sum_{m=0}^{M-1} S_{hm}(l) e^{\mathrm{j}mu_p} e^{\mathrm{j}n\nu_p} + \Xi_{hn}(l), \end{aligned} \tag{9}$$

where $\Xi_{hn}(l) = \frac{2}{L}\sum_{i=L/2}^{L-1}[\mathbf{n}_h(i)]_n e^{-\mathrm{j}\frac{2\pi i l}{L}}$ and $[\mathbf{n}_h(i)]_n$ denotes the n-th entry of $\mathbf{n}_h(i)$ given in (6). In (9), $S_{hm}(l)$ is the DFT of $\tilde{s}_{hm}(i)$, as given by

$$\begin{aligned} S_{hm}(l) &= \frac{2}{L}\sum_{i=L/2}^{L-1} F_{hm} s_{hm}(i-L_\eta) e^{-\mathrm{j}\frac{2\pi i l}{L}} \\ &= \frac{F_{hm}\sin\frac{\pi}{2}(l-k_{hm}\Delta)}{\frac{L}{2}\sin\frac{\pi}{L}(l-k_{hm}\Delta)} e^{\mathrm{j}\frac{\pi(3L-2)(k_{hm}\Delta-l)}{2L}} e^{-\mathrm{j}\frac{2\pi k_{hm}\Delta L_\eta}{L}}, \end{aligned} \tag{10}$$

where $\tilde{s}_{hm}(i)$ is replaced with $F_{hm}s_{hm}(i-L_\eta)$ based on (7).

Based on the results of the special DFT, we can also extract the signal transmitted by each antenna without inter-antenna interference, as developed in the following proposition.

Proposition 1: *Provided that the following condition holds,*

$$k_{hm}\Delta/2 \in \{0, \mathbb{I}_+\}, \ \forall m \tag{11}$$

the inter-antenna interference is also suppressed in the inter-hop interference-free signal obtained in (9). This enables the extraction of the information-bearing signal that is solely related to the m-th radar transmitter antenna at any hop h, given by

$$\begin{aligned} &Y_{hn}(l^*_{hm}) = \rho_{nm} F_{hm} e^{-\mathrm{j}\frac{2\pi L_\eta l^*_{hm}}{L}} + \Xi_{hn}(l^*_{hm}), \\ &\text{s.t.} \ \ \rho_{nm} = \sum_{p=0}^{P-1}\beta_p e^{\mathrm{j}mu_p} e^{\mathrm{j}n\nu_p}; \ l^*_{hm} = k_{hm}\Delta \end{aligned} \tag{12}$$

where Δ is given in (2), and ρ_{nm} depicts the channel coefficient between the m-th radar transmitter antenna and the n-th UE receiver antenna.

Proof: Referring to Fig. 1(b), we notice that the second half of each sampled hop is free of inter-hop interference. Since the special DFT performed in (9) only relies on the second half of each sampled hop, $Y_{hn}(l)$ obtained in (9) and $S_{hm}(l)$ calculated in (10) are also free of inter-hop interference. To this end, we focus on proving the suppression of inter-antenna interference in the rest of the proof.

Note that both sine functions in (10) take zero at $l = k_{hm}\Delta$. Thus, applying the L'Hospital's rule, we obtain,

$$S_{hm}(l^*_{hm}) = F_{hm} e^{-\mathrm{j}\frac{2\pi L_\eta l^*_{hm}}{L}}, \ \text{s.t.} \ l^*_{hm} = k_{hm}\Delta, \tag{13}$$

Also note from (10) that the signal transmitted by antenna m', $\forall m' \neq m$, has the following DFT magnitude at $l = l^*_{hm}$,

$$|S_{hm'}(l^*_{hm})| = \frac{|\sin\frac{\pi}{2}(l^*_{hm} - k_{hm'}\Delta)|}{\frac{L}{2}|\sin\frac{\pi}{L}(l^*_{hm} - k_{hm'}\Delta)|}, \ \forall m' \neq m. \tag{14}$$

To avoid inter-antenna interference, we expect the numerator on the RHS of the equation given above is zero while the denominator is non-zero. This leads to the condition given in (11). Applying the condition in (14), we obtain $|S_{hm'}(l^*_{hm})| = 0$, since its numerator is zero while the denominator is non-zero. Thus, under the condition (11), substituting (13) and (14) into (9) leads to (12). This concludes the proof. ∎

Given k_{hm} in (1) and Δ in (2), we can have the condition in (11) satisfied by configuring one of the following:

1) Take even-indexed sub-bands as hopping frequencies at hop h, i.e., $k_{hm} \in \{0, 2, 4, \cdots\}$;
2) Properly design T and K such that $\Delta/2 \in \mathbb{I}_+$.

The configuration 1) restricts the hopping frequencies available to use in a certain number of radar hops (which is M in the methods to be proposed). On the other hand, 2) can increase the hop duration and consequently reduces the number of radar hops per pulse. More in-depth analysis of the impact incurred by (11) on an FH-MIMO radar can be carried out employing the range ambiguity functions derived in [14], [23]. We proceed with the assumption that (11) is satisfied so as to focus on developing the multi-antenna receiving scheme for FH-MIMO DFRC.

Remark 1 (Insights Drawn from Proposition 1): Several insights can be drawn from Proposition 1. *First*, inter-hop and inter-antenna interference can be suppressed at a UE even in the presence of timing offset, which owes to the special DFT provided in (10) and the condition on radar waveform imposed in (11). *Second*, a clearer signal structure is obtained in (12),

as compared with (6). Specifically, the channel of FH-MIMO DFRC is now depicted by $\rho_{nm}e^{-\mathrm{j}\frac{2\pi L_\eta l^*_{hm}}{L}}$, which becomes an $M \times N$ flat-fading MIMO channel without the exponential term. Given a non-zero L_η, the channel $\rho_{nm}e^{-\mathrm{j}\frac{2\pi L_\eta l^*_{hm}}{L}}$ varies fast over hops and antennas, since l^*_{hm} randomly changes over h and m. *Third*, noticing the non-trivial impact of l^*_{hm} on the time-varying channel, we propose to explore the degrees of freedom in the FH-MIMO radar waveform for the efficient estimations of L_η and ρ_{nm}. This will be developed next.

IV. Proposed Methods

In light of the insights drawn in Remark 1, we develop a multi-antenna receiving scheme for FH-MIMO DFRC with the following tasks performed in sequence: 1) Estimate ρ_{nm}; 2) Estimate L_η; 3) Apply the estimates for information demodulation. The three tasks will be accomplished in Sections IV-A, IV-B and IV-C, respectively.

A. Estimating ρ_{nm}

At this stage, the timing offset still exists. Thus, the signal derived in (12) is used for estimating ρ_{nm}. As seen therein, $F_{hm}e^{-\mathrm{j}\frac{2\pi L_\eta l^*_{hm}}{L}}$ is a disturbance term. Nevertheless, we notice that by taking $k_{hm} = 0$, the exponential term turns into unit, since $l^*_{hm} = k_{hm}\Delta = 0$ according to (12). Accordingly, we propose the following method for estimating ρ_{nm}.

Lemma 1: *By designating the zero-th sub-band as hopping frequency in the following manner*

$$k_{hm} = 0,\ h = m,\ m = 0, 1, \cdots, M-1, \tag{15}$$

and correspondingly setting $F_{hm} = 1$, the channel coefficient between radar transmitter antenna m and UE antenna n can be estimated as

$$\hat{\rho}_{nm} = Y_{hn}(l^*_{hm}),\ h = m,\ \forall m, n, \tag{16}$$

where $Y_{hn}(l^*_{hm})$ is given in (12).

Proof: Substituting (15) into (12) yields $l^*_{hm} = 0$ and $Y_{hn}(l^*_{hm}) = \rho_{nm} + \Xi_{hn}(l^*_{hm})$ for $h = m$ ($\forall m \in [0, M-1]$). Thus, $Y_{hn}(l^*_{hm})$ can be used as an estimate of ρ_{nm}. ■

The scheduling of the zero-th hopping frequency, as given in (15), is also illustrated in Fig. 1(c). We remark that the constraint may only involve altering the pairing between hopping frequencies and antennas, and it incurs no change to the range ambiguity function according to [19, Proposition 1]. To be more specific, if there are M hops in a radar pulse having the zero-th sub-band selected originally, then we can re-assign the zero-th sub-band in such a manner that the M radar transmitter antennas can each take the zero-th sub-band over the M (non-consecutive) hops. If there are less than M hops selecting the zero-th sub-band as hopping frequency, then we need to insert the zero-th sub-band to some hops to make the number of such hops becomes M. Given that an FH-MIMO radar randomly selects hopping frequencies to use [23], the insertion can have negligible impact on the range ambiguity function of the radar.

B. Estimating L_η

Using the estimate $\hat{\rho}_{nm}$, we can obtain an equivalent channel coefficients from (12), leading to

$$\tilde{Y}_{hnm} = \frac{Y_{hn}(l^*_{hm})}{\hat{\rho}_{nm}} = e^{-\mathrm{j}\frac{2\pi L_\eta l^*_{hm}}{L}} + \tilde{\Xi}_{hnm}, \tag{17}$$

where $\tilde{\Xi}_{hnm} = \Xi_{hn}(l^*_{hm})/\hat{\rho}_{nm}$. Note that the exponential term becomes the same for all the UE antennas, and hence we can coherently combine $\tilde{Y}_{hnm}$ over n to improve the estimation SNR. This yields

$$\bar{Y}_{hm} = \frac{1}{N}\sum_{h=0}^{N-1}\tilde{Y}_{hnm} = e^{-\mathrm{j}\frac{2\pi L_\eta \Delta k_{hm}}{L}} + \bar{\Xi}_{hm}, \tag{18}$$

where l^*_{hm} is replaced by $k_{hm}\Delta$ given their relation in (12), and $\bar{\Xi}_{hm} = \frac{1}{N}\sum_{n=0}^{N-1}\tilde{\Xi}_{hnm}$. To estimate L_η, we propose to transform the timing offset estimation problem as follows.

Lemma 2: *Design the hopping frequencies at hop $h = 0$ such that they take continuous values, e.g.,*

$$k_{0m} = k_0 + m,\ m = 0, 1, \cdots, M-1, \tag{19}$$

where k_0 can take 0 or any integer from $\{1, \cdots, K-M\}$. Then, we can turn the L_η estimation into a more tractable problem which estimates the frequency, denoted by Υ, of a discrete single-tone signal,

$$\bar{Y}_{0m} = e^{-\mathrm{j}\frac{2\pi\Upsilon k_0}{M}}e^{-\mathrm{j}\frac{2\pi\Upsilon m}{M}} + \bar{\Xi}_{0m},\ \text{s.t. } \Upsilon = L_\eta\Delta M/L. \tag{20}$$

The proof can be established by substituting (19) into (18) and reshaping the exponent of the exponential term. Clearly, the single-tone frequency estimation problem, as formulated in Lemma 2 is more tractable, compared with estimating L_η based on (18). However, there can be an estimation ambiguity problem, as elaborated on below. According to the definition of Υ given in (20), we have $\Upsilon \in [0, \Delta M/2]$. That is, $\Upsilon > M$ can happen if $\Delta > 2$. Given the up limit of Υ, we have $\Upsilon/M = \Delta/2$. Thus, we can express Υ as

$$\Upsilon = (\Upsilon)_M + dM,\ \text{s.t. } d = 0, 1, \cdots, \lceil \Delta/2 \rceil - 1, \tag{21}$$

where $(\cdot)_M$ denotes modulo-M and d is referred to as the ambiguity degree. Substituting (21) into (20), we obtain

$$\bar{Y}_{0m} = e^{-\mathrm{j}\frac{2\pi\Upsilon k_0}{M}}e^{-\mathrm{j}\frac{2\pi(\Upsilon)_M m}{M}} + \bar{\Xi}_{0m}. \tag{22}$$

We see that only $(\Upsilon)_M$ can be estimated from $\bar{Y}_{0m}$. In other words, Υ can be estimated from $\bar{Y}_{0m}$ with an ambiguity degree of d. In the following, we apply the method developed in [33] to estimate $(\Upsilon)_M$ from $\bar{Y}_{0m}$, given that the method has low computational complexity and high accuracy. We will also design the method to recover Υ from $(\Upsilon)_M$.

1) Estimating L_η: A coarse estimate of Υ can be obtained from the DFT of $\bar{Y}_{0m}$ w.r.t. m which is given by

$$\mathsf{Y}_m = \frac{1}{M}\sum_{m'=0}^{M-1}\bar{Y}_{0m'}e^{-\mathrm{j}\frac{2\pi m' m}{M}}.$$

Let $\tilde{m}$ denote the peak index of $|\mathsf{Y}_m|$, and then a coarse estimate of $(\Upsilon)_M$ is given by $\frac{2\pi\tilde{m}}{M}$. While the actual value of $(\Upsilon)_M$ can be expressed as $\frac{2\pi(\tilde{m}+\delta)}{M}$, with $\delta \in [-0.5, 0.5]$ denoting the fractional part of $(\Upsilon)_M$.

Next, we iteratively interpolate the DFT coefficients around $\tilde{m}$ to estimate δ [34].

Step 1) Compute the interpolated DFTs as follows

$$\mathsf{Y}_{\pm} = \frac{1}{M}\sum_{m'=0}^{M-1} Y_{0m'} e^{-\mathrm{j}\frac{2\pi m'(\tilde{m}+\delta\pm\epsilon)}{M}}, \tag{23}$$

where δ (to be updated) takes zero initially, i.e., $\delta = 0$, and ϵ is a constant intermediate variable which takes $\epsilon = \min\{M^{-\frac{1}{3}}, 0.32\}$ [33, Eq. (23)].

Step 2) Set $\delta_{\text{old}} = \delta$ and update δ as follows [34]

$$\delta = \frac{\epsilon\cos^2(\pi\epsilon)}{1-\pi\epsilon\cot(\pi\epsilon)} \times \Re\{\zeta\} + \delta_{\text{old}}, \tag{24}$$

where $\zeta = \frac{\mathsf{Y}_+ - \mathsf{Y}_-}{\mathsf{Y}_+ + \mathsf{Y}_-}$ is calculated based on (23).

Step 3) Iteratively perform the above two steps for up to N_{iter} rounds. The final δ is given by $\delta^* = \delta_{N_{\text{iter}}}$

In general, $N_{\text{iter}} = 3$ enables the algorithm to converge [33], [34], with the convergent performance approaching the CRLB to be derived in Section V-B. The estimate of $(\Upsilon)_M$ is given by $(\tilde{m} + \delta^*)$, thus, based on (21), the final estimate of Υ is

$$\hat{\Upsilon} = \tilde{m} + \delta^* + dM,\ d = 0, 1, \cdots, \lceil \Delta/2 \rceil - 1. \tag{25}$$

Substituting (25) into (20), we obtain the estimate of L_η, as given by

$$\hat{L}_\eta^{(d)} = L(\tilde{m} + \delta^*)/(M\Delta) + Ld/\Delta. \tag{26}$$

2) Removing Estimation Ambiguity: We enumerate the possible estimates and compare the SNR in the recovered hops, since the ambiguity degree is generally limited given the potentially small value of Δ. Besides, we use the first hop to fulfill the task, given that it has a known feature; see Lemma 2. Based on (6) and (7), the first "complete" hop, recovered using $\hat{L}_\eta^{(d)}$, is given by

$$y_{0n}^{(d)}(i) = \Big[y_{0n}(\hat{L}_\eta^{(d)}), \cdots, y_{0n}(L-1), y_{1n}(0), \cdots, y_{1n}(\hat{L}_\eta^{(d)} - 1)\Big]^{\mathrm{T}}, \tag{27}$$

where $y_{hn}(i)$ $(h = 0, 1)$ is the n-th entry of $\mathbf{y}_h(i)$ given in (6) and $y_{0n}^{(d)}(i)$ denotes the recovered first hop. Take the L-point DFT of $y_{0n}^{(d)}(i)$, leading to

$$X_{0n}^{(d)}(l) = \frac{1}{L}\sum_{i=0}^{L-1} y_{0n}^{(d)}(i) e^{-\mathrm{j}\frac{2\pi i l}{L}}. \tag{28}$$

Provided that d^* is the correct ambiguity degree and $\hat{L}_\eta^{(d^*)}$ is sufficiently accurate, $X_{0n}^{(d^*)}(l)$ becomes

$$X_{0n}^{(d^*)}(l) = \sum_{p=0}^{P-1}\beta_p e^{\mathrm{j}n\nu_p}\sum_{m=0}^{M-1} e^{\mathrm{j}mu_p}\delta(l - l_{0m}^*) + \Pi_{hn}(l).$$

As a result, there are only M effective values in $X_{0n}^{(d^*)}(l)$ as given by $X_{0n}^{(d^*)}(l_{0m}^*) = \rho_{nm} + \Pi_{0n}(l_{0m}^*)$ $(m = 0, 1, \cdots, M-1)$, where ρ_{nm} is given in (12). The rest of $X_{0n}^{(d^*)}(l)$ $(l \neq l_{0m}^*)$ are noises. Therefore, the SNR of a correctly recovered hop can be given by

$$\gamma_{X_0}^{(d^*)} = \frac{\frac{1}{MN}\sum_{m=0}^{M-1}\sum_{n=0}^{N-1}|X_{0n}^{(d^*)}(l_{0m}^*)|^2}{\frac{1}{N(L-M)}\sum_{\substack{l=0\\ l\neq l_{0m}^*}}^{L-1}\sum_{n=0}^{N-1}|X_{0n}^{(d^*)}(l)|^2}. \tag{29}$$

For $d \neq d^*$, part of the signal power will leak to the sidelobe region, incurring a decrease of the numerator and an increase of the denominator in $\gamma_X^{(d^*)}$. Therefore, the correct ambiguity degree can be identified via solving the following problem

$$d^* = \text{argmax}_{d=0,1,\cdots,\lceil\Delta/2\rceil-1}\ \gamma_{X_0}^{(d)}, \tag{30}$$

where $\gamma_{X_0}^{(d)}$ is calculated by replacing $X_{0n}^{(d^*)}(l)$ in (29) with $X_{0n}^{(d)}(l)$ obtained in (28).

Remark 2: We remark that the overall complexity of the proposed methods is generally low, as analyzed below. The complexity of the estimation of ρ_{nm} developed in Section IV-A is dominated by computing $Y_{hn}(l)$, as given in (9). The complexity of this computation can be given by $\mathcal{O}(MNL^2)$, where the factor M is because the computation happens over M hops; see Lemma 2, and N is because the computation needs to be performed for each of the N receiver antennas. The complexity of estimating L_η, as developed in Section IV-B, is dominated by the computations in (17), (23) and (30). Their complexities can be, respectively, given by $\mathcal{O}(MN)$, $\mathcal{O}(2I_{\text{iter}}M)$ and $\mathcal{O}(\lceil\Delta/2\rceil L\log_2 L)$, where I_{iter} is the number of iterations performed for estimating $(\Upsilon)_M$ from $\bar{Y}_{0m}$. As mentioned earlier, $I_{\text{iter}} = 3$ ensures asymptotic convergence to the CRLB. Jointly considering the complexity in the four $\mathcal{O}(\cdot)$ expressions given above, the overall computational complexity of the proposed scheme is in the order of $\mathcal{O}(MNL^2)$.

C. Information Demodulation

With L_η estimated and compensated, we can take the standard L-dimensional DFT of $y_{hn}(i)$ $(\forall h \geq 2)$ given in (6), leading to

$$\begin{cases} Z_{hn}(l) = \frac{1}{L}\sum_{i=0}^{L-1} y_{hn}(i) = \sum_{p=0}^{P-1}\beta_p e^{\mathrm{j}n\nu_p} \times \\ \qquad \sum_{m=0}^{M-1} e^{\mathrm{j}mu_p}\delta(l - l_{hm}^*) F_{hm} + \Pi_{hn}(l); \\ Z_{hn}(l_{hm}^*) = \rho_{nm}F_{hm} + \Pi_{hn}(l_{hm}^*), \end{cases} \tag{31}$$

where $\Pi_{hn}(l) = \frac{1}{L}\sum_{i=0}^{L-1}[\mathbf{n}_h(i)]_n e^{-\mathrm{j}\frac{2\pi i l}{L}}$. To demodulate F_{hm}, we need extract the signal component solely associated with the m-th radar transmitter antenna, i.e., $Z_{hn}(l_{hm}^*)$ given in (31). However, the index $l_{hm}^* = k_{hm}\Delta$ needs to estimated, which essentially requires the estimation of k_{hm} (the hopping frequency used by antenna m at hop h).

1) Estimating k_{hm}: Conventional FH-MIMO radars can randomly change hopping frequencies over hops [23]. To make it possible for the UE to estimate k_{hm}, we propose to re-pair the hopping frequencies with radar transmitter antennas at each hop. Specifically, after hopping frequencies are randomly selected for a hop, the frequencies are sorted in an ascending order before assigned to the antennas. This leads to

$$\begin{cases} k_{hm} < k_{h(m+1)} & h \in [1, M-1],\ \forall m,\ m \neq h \\ k_{hm} < k_{h(m+1)} & h \in [M, H-1],\ \forall m, \end{cases} \tag{32}$$

TABLE I
ESTIMATING k_{hm}

1) Use $\hat{L}_{\eta}^{(d^*)}$ to remove the timing offset and re-construct hop h $(\forall h > 0)$, as done in (27), where the subscripts 0 and 1 are replaced by h and $(h+1)$, respectively;
2) Take the standard L-point DFT of the reconstructed hops, leading to $Z_{hn}(l)$ given in (31);
3) To exploit the antenna diversity, we can combine $Z_{hn}(l)$ over $\forall n$, which gives $\bar{Z}_h(l) = \frac{1}{N}\sum_{n=0}^{N-1}|Z_{hn}(l)|^2$; refer to Remark 3 for the illustration of diversity gain.
4) Identify the strongest M peaks from $\bar{Z}_h(l)$ with the peak indexes denoted by $l_{m'}$ $(l_0 < l_1 < \cdots < l_{(M-1)})$;
5) Associate the peaks with the radar transmitter antennas based on (32), leading to the estimates of k_{hm} and $l_{hm}^*(= k_{hm}\Delta)$, denoted by $\hat{k}_{hm}$ and $\hat{l}_{hm}^*$, respectively.

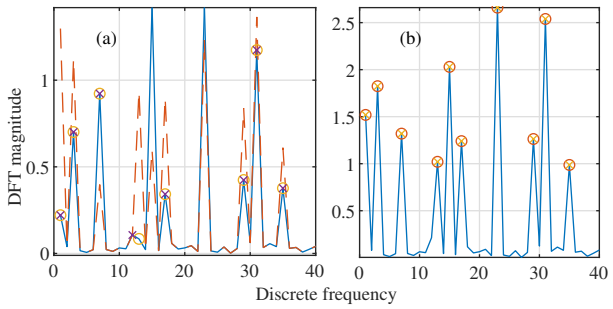

Fig. 2. Illustration of signal cancellation. In Fig. 2(a) the solid curve is for $|Z_{h0}(l)|$ and the dash for $|Z_{h1}(l)|$. In Fig. 2(b), the solid curve plots $|\bar{Z}_h(l)|$. In both figures, circular markers indicate the set hopping frequencies and cross markers the detected. Here, $N = 2$ and the other parameters are the same as those used in Section VI.

where $m \neq h$ in the first row is to enforce condition (15) required in Lemma 1. As assured by [19, Proposition 1], the above re-pairing does not incur any change to the radar range ambiguity function. Enabled by (32), we propose to identify the hopping frequencies, as summarized in Table I.

Remark 3: The information-bearing signal from the m-th radar transmitter antenna can be severely attenuated when arriving at the UE. This can be seen from the complex summation of multiple paths, i.e., $\sum_{p=0}^{P-1}\beta_p e^{\mathrm{j}mu_p}e^{\mathrm{j}n\nu_p}F_{hm}$ given in (12) and (31). The phenomenon, referred to as *signal cancellation*, can severely degrade the detection performance of $\hat{k}_{hm}$. As demonstrated in Fig. 2(a), the fourth DFT peak is attenuated severely such that it is missed. From (12) and (31), we notice that if $\sum_{p=0}^{P-1}\beta_p e^{\mathrm{j}mu_p}e^{\mathrm{j}n\nu_p}F_{hm}$ approaches zero, it is likely that $\sum_{p=0}^{P-1}\beta_p e^{\mathrm{j}mu_p}e^{\mathrm{j}n'\nu_p}F_{hm} \gg 0$ for some $n' \neq n$ since the phase $n\nu_p$ $(\forall \nu_p \neq 0)$ varies with n. The antenna diversity can be exploited to reduce the effect of signal cancellation, as performed in Step 3) of Table I. The efficacy of the combining in Step 3) is demonstrated by Fig. 2(b). We see that the magnitudes of DFT peaks are substantially enhanced, with only two antennas at the UE.

2) FHCS Demodulation: Note that the combinations of k_{hm} $\forall m$ at any hop can be used for information modulation, which is referred to as frequency hopping code selection (FHCS) [18]. Given K available sub-bands and M transmitter antennas at the radar, there can be C_K^M combinations of hopping frequencies. We can select $2^{J_{\mathrm{FHCS}}}$ combinations as constellation points which can convey $J_{\mathrm{FHCS}} = \lfloor \log_2\left(C_K^M\right)\rfloor$ bits per radar hop. Comparing $\{\hat{k}_{hm}\ \forall m\}$ with the constellation points can demodulate the FHCS symbol, where $\hat{k}_{hm}$ $\forall m$ is obtained from Step 5) in Table I.

3) PSK Demodulation: With $\hat{l}_{hm}^*$ $\forall m$ estimated using the method given in Table I, we can extract the M values of $Z_{hn}(l)$ at $\hat{l}_{hm}^*$, attaining $Z_{hn}(\hat{l}_{hm}^*)$ which has the same structure as $Z_{hn}(l_{hm}^*)$. Then we use the ρ_{nm} estimates obtained in Lemma 1 to perform MRC over UE antennas. This yields

$$\tilde{Z}_{hm} = \left(\sum_{n=0}^{N-1}\hat{\rho}_{nm}^* Z_{hn}(\hat{l}_{hm}^*)\right) \Big/ \left(\sum_{n=0}^{N-1}|\hat{\rho}_{nm}|^2\right). \quad (33)$$

Finally, $\tilde{Z}_{hm}$ can be used for demodulating F_{hm}. We remark that the enabling factors for exploiting antenna diversity, as done in Step 3) of Table I and (33), are non-trivial. In particular, they are enabled by the accurate estimations of channel responses and timing offset obtained in Sections IV-A and IV-B, respectively. Moreover, these estimation methods are developed on the basis of our insights into the UE-received signals in the FH-MIMO DFRC, as illustrated in Section III.

V. PERFORMANCE ANALYSIS

The performance of the proposed estimation and demodulation methods is analyzed in this section.

A. Performance of Channel Coefficient Estimation

We first analyze the performance of the proposed estimation method for channel coefficients. In particular, we derive the following analytical MSE of $\hat{\rho}_{nm}$ achieved in Lemma 1.

Corollary 1: *The analytical MSE of $\hat{\rho}_{nm}$ is given by*

$$\sigma_{\hat{\rho}_{nm}}^2 = 2\sigma_0^2/L,\ \forall n, m, \quad (34)$$

where σ_0^2 is the power of each entry of $\mathbf{n}_h(i)$ given in (6).

Proof: Given (15) and $F_{hm} = 1$, $Y_{hn}(l_{hm}^*)$ degenerates into ρ_{nm} plus an AWGN $\Xi_{hn}(l_{hm}^*)$. Therefore, the estimation error of ρ_{nm} is $\Xi_{hn}(l_{hm}^*)$, and the noise power is the estimation MSE. Given the relation between $\mathbf{n}_h(i)$ and $\Xi_{hn}(l)$; see below (6), the noise power of the later is $2\sigma_0^2/L$, so is the MSE of $\hat{\rho}_{nm}$. ■

From Corollary 1, we see that the estimation performance of ρ_{nm} is solely related to the number of samples in a radar hop, i.e., L , and the variance of the antenna-level noise, i.e., σ_0^2. This manifests the applicability of the proposed channel estimation method in various channel models. It is worth pointing out that the flexible applicability is achieved by the novel waveform design, as given in (15).

B. Performance of Timing Offset Estimation

To evaluate the performance of the proposed estimation method for timing offset, we derive the CRLB of $L_{\eta}^{(d^*)}$.

Proposition 2: *Provided that NLoS paths are negligible compared with the LoS path and $\hat{\rho}_{nm}$ approaches its true value ρ_{nm}, the CRLB of $L_\eta^{(d^*)}$ is given by*

$$\mathrm{CRLB}\left\{L_\eta^{(d^*)}\right\} = \frac{3L}{\pi^2 M^3 N \Delta^2 \gamma_0}, \tag{35}$$

where $\gamma_0 = \frac{|\beta_0|^2}{\sigma_0^2}$, β_0 is the complex gain of the LoS path and σ_0^2 is given in Corollary 1.

Proof: According to [34], the CRLB of estimating Υ from $\gamma_{\bar{Y}}$ given in (20) can be expressed as $\frac{6}{4\pi^2 M \gamma_{\bar{Y}}}$, where $\gamma_{\bar{Y}}$ is the SNR in $\bar{Y}_{0m}$. Based on relation between Υ and L_η illustrated in (20), the CRLB of L_η estimate can be given by

$$\mathrm{CRLB}\left\{L_\eta^{(d^*)}\right\} = \frac{6L^2}{4\pi^2 M^3 \Delta^2 \gamma_{\bar{Y}}}. \tag{36}$$

Next, we derive $\gamma_{\bar{Y}}$ for the CRLB.

Given (20), we have $\gamma_{\bar{Y}} = 1/\sigma_{\bar{\Xi}}^2$, where $\sigma_{\bar{\Xi}}^2$ denotes the noise variance of $\bar{\Xi}_{0m}$. Based on (18), we obtain $\sigma_{\bar{\Xi}}^2 = \frac{1}{N}\sigma_{\tilde{\Xi}}^2$, where $\sigma_{\tilde{\Xi}}^2$ is the noise variance of $\tilde{\Xi}_{0nm}$ give in (17). We can derive from (17) that $\sigma_{\tilde{\Xi}}^2 = \frac{1}{|\hat{\rho}_{nm}|^2}\sigma_{\Xi}^2 \approx \frac{1}{|\beta_0|^2}\sigma_{\Xi}^2$, where the last approximation is based on the claimed conditions of Proposition 2, and σ_{Ξ}^2 is the noise power of $\Xi_{0n}(l_{0m}^*)$ given in (9). As derived in the Corollary 1, $\sigma_{\Xi}^2 = 2\sigma_0^2/L$. Backtracking the above changes of noise components, we obtain $\gamma_{\bar{Y}} = \frac{LN\gamma_0}{2}$. Substituting this into (36) leads to (35), which concludes the proof. ∎

From Proposition 2, we see that the performance of the proposed timing offset estimation method is inversely proportional to the third power of M and the first power of N. This indicates that increasing M, rather than N, can be more effective in achieving better L_η estimation (and hence better communication performance). Note that the L-dependence shown in (35) is not straightforward, since Δ in the denominator is also related to L. Taking $f_\mathrm{s} = 2B$, we have $\Delta = BT/K = L/(2K)$ based on (2). Substituting this into (35) leads to

$$\mathrm{CRLB}\left\{L_\eta^{(d^*)}\right\} = \frac{12K^2}{\pi^2 M^3 N L \gamma_0}, \tag{37}$$

where we see that the estimation performance can be improved by increasing L. This complies with the fact that a larger L corresponds to a greater DFT dimension and hence a larger estimation SNR, as analyzed in the proof of Proposition 2.

C. Communication Performance

We proceed to analyze the communication performance of FH-MIMO DFRC achieved by the proposed receiving scheme.

1) Achievable Rate: The symbol rate of FH-MIMO DFRC is given by H/T_PRT (symbol/second), where T_PRT denotes the pulse repetition interval of the FH-MIMO radar. Thus, the achievable rate of FH-MIMO DFRC can be given by

$$\mathsf{R}_\mathrm{DFRC} = \frac{HJ}{T_\mathrm{PRT}} = \mathsf{r}J/T, \tag{38}$$

where J denotes the number of bits conveyed in each radar hop, r the duty cycle and T the hop duration. Based on (5), we have $J = MJ_\mathrm{PSK}$ and hence $\mathsf{R}_\mathrm{PSK} = \mathsf{r}MJ_\mathrm{PSK}/T$. Based on Section IV-C2, we have $J = J_\mathrm{FHCS} = \lfloor \log_2\left(C_K^M\right) \rfloor$ and hence $\mathsf{R}_\mathrm{FHCS} = \mathsf{r}\lfloor \log_2\left(C_K^M\right) \rfloor/T$.

From (38), we see that reducing T can help improve the achievable rate. This, however, may not stand for the FHCS-based FH-MIMO DFRC, since J_FHCS is related to T. According to (2), a smaller T results in a smaller $\Delta(= BT/K)$. To keep (11) satisfied at a fixed B, we need to reduce K. Moreover, a smaller K can yield a smaller $\lfloor \log_2\left(C_K^M\right) \rfloor$ given a fixed M. Therefore, reducing T can lead to the decreases of both the numerator and denominator of R_FHCS. Note that the system parameters can be holistically designed to optimize the performance (trade-off) of radar and communications under the proposed receiving scheme. This is left for future work.

2) SER of PSK-based FH-MIMO DFRC: Note that a DFRC symbol consists of M PSK sub-symbols, i.e., F_{hm}, $m = 0, 1, \cdots, M-1$, each from a radar transmitter antenna. To this end, the h-th DFRC symbol is correctly demodulated only when each F_{hm} $\forall m$ is correctly demodulated. Consider Rician channel here. The resultant performance analysis can be readily extended to Rayleigh or AWGN channel by varying the Rician factor K. According to Section IV-C3, F_{hm} $\forall m$ is independently demodulated over identically distributed Rician channels, the SER of demodulating F_{hm} $\forall m$ is identical and denoted by $\tilde{\mathsf{P}}_\mathrm{PSK}$.

From (33), we see that F_{hm} $\forall m$ is demodulated from the MRC over N antennas with the spacing of half a wavelength. Thus, the identically distributed Rician channels over the N antennas can be highly correlated. To avoid the complexity of analysis incurred by the channel coherence [35], we proceed to derive the lower bound of $\tilde{\mathsf{P}}_\mathrm{PSK}$ by treating the MRC result as a single Rician channel with the identical distribution yet an N-fold SNR improvement, compared with the Rician channel on a single UE receiver antenna. Applying the SER of PSK demodulation in a Rician channel, as derived in [36], we obtain

$$\begin{aligned}\underline{\tilde{\mathsf{P}}}_\mathrm{PSK} &= \int_0^{\frac{\pi}{2}} \frac{e^{-\mathsf{K}+\frac{\mathsf{K}}{\Omega(\theta)}}}{\pi\Omega(\theta)}\,\mathrm{d}\theta + \int_0^{\frac{\pi}{2}-\frac{\pi}{J_\mathrm{PSK}}} \frac{e^{-\mathsf{K}+\frac{\mathsf{K}}{\Omega(\theta)}}}{\pi\Omega(\theta)}\,\mathrm{d}\theta,\\ &\text{s.t. } \Omega(\theta) = 1 + \frac{LN\gamma_0 \sin^2\frac{\pi}{J_\mathrm{PSK}}}{\mathsf{K}\cos^2\theta},\end{aligned} \tag{39}$$

where γ_0 is the antenna-level SNR defined in Proposition 2. Accordingly, the SER of demodulating M PSK sub-symbols is lower-bounded by

$$\underline{\mathsf{P}}_\mathrm{PSK} = 1 - \left(1 - \underline{\tilde{\mathsf{P}}}_\mathrm{PSK}\right)^M, \tag{40}$$

where $(1-\underline{\tilde{\mathsf{P}}}_\mathrm{PSK})^M$ gives the probability of correctly detecting the M PSK sub-symbols in a radar hop.

VI. Simulations

In this section, we validate the proposed design through extensive simulations. Unless otherwise specified, we employ the following parameters, where the FH-MIMO radar is configured with refer to [18]: $\mathsf{r} = 0.2$, $B = 100$ MHz, $f_\mathrm{s} = 2B$, $K = 20$, $M = H = 10$, $N = 6$, $T = 0.4\mu$s (hence $L = f_\mathrm{s}T = 80$ and $\Delta = BT/K = 2$), and $L_\eta \in \mathcal{U}_{[0,L/2]}$ with $\mathcal{U}_{[a,b]}$ denoting the uniform distribution in $[a, b]$. Applying the parameters in Section V-C1, we obtain

$$\mathsf{R}_\mathrm{PSK} = 0.2 \times 10/(0.4 \times 10^{-6}) = 5 \text{ Mbps};$$

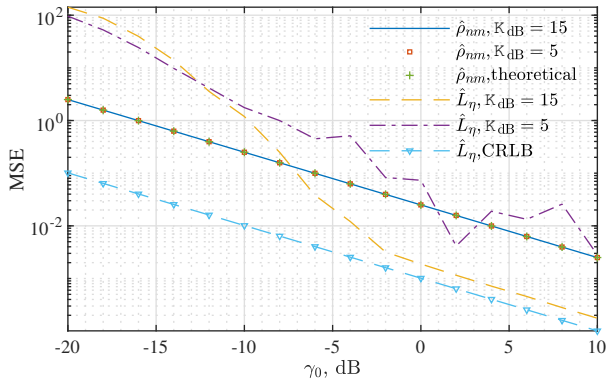

Fig. 3. MSE of $\hat{\rho}_{nm}$ obtained in (16) and $\hat{L}_\eta^{(d^*)}$ given in (26).

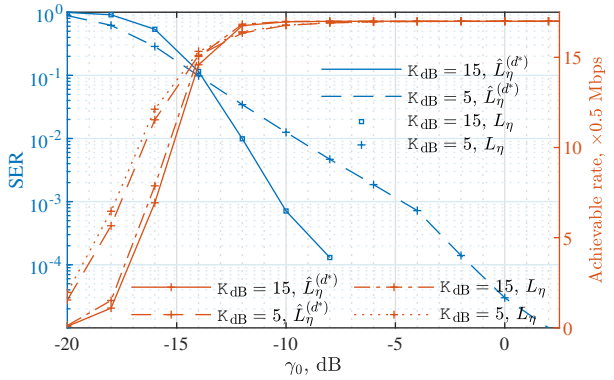

Fig. 4. Communication performance of FHCS-based FH-MIMO DFRC against γ_0, where the curves with "+" markers use the y-axis on the right.

$$\mathsf{R}_{\rm FHCS} = 0.2 \times \lfloor \log_2 \left(C_{20}^{10}\right) \rfloor / (0.4 \times 10^{-6}) = 8.5 \text{ Mbps}.$$

As for communication scenarios, the Rician channel with an LoS and three NLoS paths is simulated, i.e., $P = 4$, where $\theta_p \in \mathcal{U}_{[-90^\circ,90^\circ]}$ $\forall p$, $\phi_p \in \mathcal{U}_{[-90^\circ,90^\circ]}$ $\forall p$, $\beta_0 = e^{\mathrm{j}x}$ with $x \in \mathcal{U}_{[0,2\pi]}$, and $\beta_p \sim \mathcal{CN}(0, \mathsf{K}_{\rm dB})$ $(\forall p \in [1, P-1])$ with $\mathsf{K}_{\rm dB} = -\log_{10} \frac{\mathsf{K}}{P-1}$ denoting the Rician factor in decibel. Below, $\gamma_0 = \frac{|\beta_0|}{\sigma_0^2}$ represents the antenna-level SNR at the UE.

Fig. 3 plots the MSE of $\hat{\rho}_{nm}$ and $\hat{L}_\eta$ against γ_0, where both $\mathsf{K}_{\rm dB} = 15$ dB and 5 dB are considered. In terms of $\hat{\rho}_{nm}$, we see that the simulated MSE of $\hat{\rho}_{nm}$ monotonically decreases with γ_0 and coincides with the analytical MSE derived in Corollary 1. This validates the ρ_{nm} estimation method proposed in Section IV-A. We also see that the MSE of $\hat{\rho}_{nm}$ is invariant under different values of $\mathsf{K}_{\rm dB}$. This is because we can fully decouple the estimations of ρ_{nm} and L_η, making the estimation error of $\hat{\rho}_{nm}$ solely dependent on background noises; see Section IV-A.

As for $\hat{L}_\eta$, we see from Fig. 3 that, at $\mathsf{K}_{\rm dB} = 15$ dB, the MSE of $\hat{L}_\eta$ approaches the CRLB derived in Proposition 2 in the region of $\gamma_0 > -2$ dB. This validates the high accuracy of the proposed L_η estimation method, particularly given a large $\mathsf{K}_{\rm dB}$. We also see from the figure that the MSE of $\hat{L}_\eta$ achieved at $\mathsf{K}_{\rm dB} = 5$ dB is not as low as that at $\mathsf{K}_{\rm dB} = 15$ dB, and fluctuates in high SNR regions. This is because the multi-path components lead to uneven noise variance across the M signals constructed for L_η estimation; see (17). Despite the slight MSE fluctuation, the overall performance of $\hat{L}_\eta$ at $\mathsf{K}_{\rm dB} = 5$ dB improves with γ_0, which is adequate for high communication performance, as illustrated subsequently.

Fig. 4 plots the SER and achievable rate of FHCS-based FH-MIMO DFRC against γ_0, where $\hat{L}_\eta^{(d^*)}$ obtained for Fig. 3 is used to remove the timing offset in the UE-received signals, as elaborated on in Section IV-C. We see that the SER curves achieved by the estimated and actual values of L_η are nearly overlapped in the observed SNR regions. This validates the proposed multi-antenna receiving scheme, as developed in Section IV and manifests its robustness against the estimation error of $\hat{L}_\eta$. We also see from Fig. 4 that, enabled by the proposed methods, the SNR required for the achievable rate of FHCS to approach $\mathsf{R}_{\rm PSK}$ with the SER of 10^{-4} is as low as $\gamma_0 = -7$ dB given $\mathsf{K}_{\rm dB} = 15$ dB, whereas the required SNR

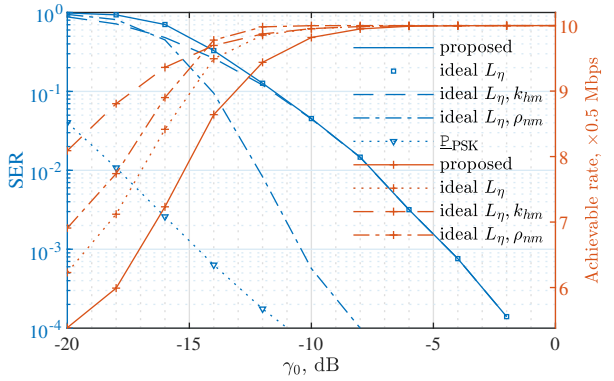

Fig. 5. Communication performance of BPSK-based FH-MIMO DFRC, with $\mathsf{K}_{\rm dB} = 15$ dB and the estimated parameters used, unless otherwise specified. The curves with "+" markers use the y-axis on the right. The SER lower bound $\underline{\mathsf{P}}_{\rm PSK}$ is given in (40).

increases to -1 dB for $\mathsf{K}_{\rm dB} = 5$ dB. The moderate increase is caused by the signal cancellation illustrated in Remark 3.

Fig. 5 plots the SER and achievable rate of BPSK-based FH-MIMO DFRC against γ_0 in the case of $\mathsf{K}_{\rm dB} = 15$ dB. We see that the proposed multi-antenna receiving scheme enables the SER of BPSK to decrease consistently over the observed region of γ_0. In particular, the SER decreases to nearly 10^{-4} at a low SNR of $\gamma_0 = -2$ dB. We also see that in the region of $\gamma_0 \leq -16$ dB, k_{hm} has a more dominant impact on the SER than ρ_{nm} and the reverse is seen in the region of $\gamma_0 > -16$ dB. From the achievable rate curves, we see that the proposed design enables BPSK-based FH-MIMO DFRC to approach $\mathsf{R}_{\rm PSK}$ once $\gamma_0 \geq -6$ dB. Moreover, the SNR required for 10^{-4} SER is as low as -1 dB.

Fig. 6 plots the SER and achievable rate of BPSK-based FH-MIMO DFRC against γ_0 in the case of $\mathsf{K}_{\rm dB} = 5$ dB. We see a decreasing SER w.r.t. γ_0. However, the decreasing rate is smaller, as compared with the large-$\mathsf{K}_{\rm dB}$ results given in Fig. 5. The main reason for this change is the SNR fluctuation across UE antennas, where the fluctuation is further caused by the different extents of signal cancellation presented on UE antennas. As for the achievable rate, we see from Fig. 6 that the SNR required for approaching 10 Mbps is -1 dB, which is 5 dB higher that observed in Fig. 5.

Figs. 5 and 6 also plot the derived SER lower bounds for BPSK-based FH-MIMO DFRC. We see that the bound can precisely depict the the actual SER performance particularly

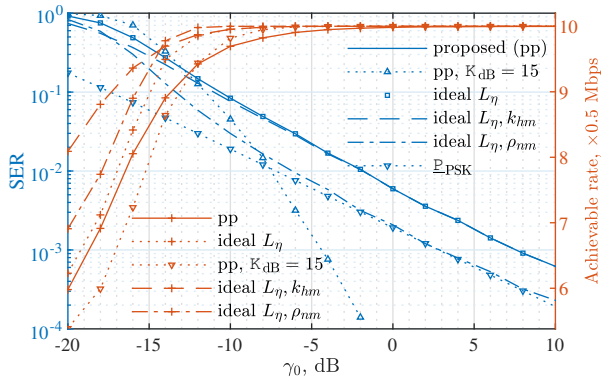

Fig. 6. The same simulation as done in Fig. 5 with $\mathsf{K}_{\rm dB} = 5$ dB here.

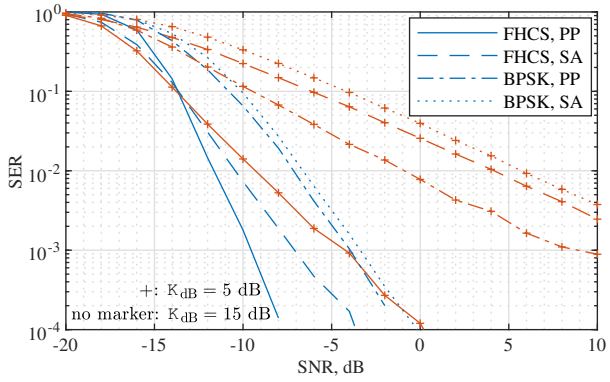

Fig. 7. Comparing SER between the proposed (PP) muli-antenna receiving scheme and the single-antenna (SA) schemes, where "FHCS, SA" and "BPSK, SA" are obtained by the methods designed in [18] and [14], respectively.

when K is small. This is because the Rician channel can degenerate into the LoS-dominant AWGN channel for large values of K. Jointly observing the two figures, we further see that between the two performance metrics, the SER is more prone to multi-path fading, as compared with the achievable rate. Precoding can be designed at the radar to enhance the SER performance. This is left for future work.

Fig. 7 compares the proposed multi-antenna receiving scheme with two single-antenna schemes designed in [18] and [14]. For fair comparison, the same multi-path fading and total transmission power are set for all schemes. Since the benchmark methods use a single antenna, their SNR is thus $10\log_{10} N$ dB higher than the proposed scheme at each receiving antenna. For example, at the SNR of 0 dB in the figure, the SNR for the two benchmark schemes is $10\log_{10} N$ dB. From Fig. 7, we see that the proposed receiving scheme substantially outperforms the benchmark schemes [14], [18], particularly when FHCS modulation is performed. Specifically, we see that to achieve a SER of 10^{-3} for FHCS, the proposed scheme only requires an SNR of -4 dB, while the scheme [18] would require an SNR larger than 10 dB. In addition, we see that the SER curves achieved by the proposed scheme are much steeper than those by the benchmark schemes, which shows the diversity gain achieved by the proposed scheme.

Fig. 8 plots the SER performance of FHCS-/BPSK-based FH-MIMO DFRC against N. We see that both FHCS and

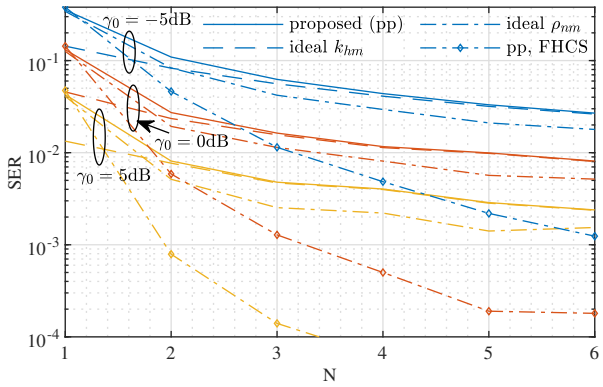

Fig. 8. SER of FH-IMMO DFRC against N, where, unless otherwise specified, $\mathsf{K}_{\rm dB} = 5$ dB, and we use BPSK and the estimated parameters.

BPSK have better SER performance as N increases. Particularly from $N = 1$ to $N = 2$, the SER decrease of FHCS can be orders of magnitude. This improvement is because the demodulation SNRs of FHCS and BPSK increase with N; see Section IV-C. We also see that N has a more evident impact on FHCS. This is because FHCS is more prone to the signal cancellation illustrated in Remark 3; hence increasing N can introduce more diversity over UE antennas. We conclude from Fig. 8 that furnishing the UE with a multi-antenna receiver can dramatically improve the performance of FH-MIMO DFRC. It is worth mentioning that the high communication performance is achieved by the proposed receiving scheme and estimation methods for channel parameters.

VII. Conclusions and Future Works

A high-performance multi-antenna receiving scheme is developed for FH-MIMO DFRC in multi-path channels. This is achieved by a special time-frequency transformation which suppresses inter-antenna and inter-hop interference, and substantially simplifies the DFRC signal model. This is also accomplished by devising new minimal constraints on radar waveform, decoupling the estimations of channel coefficients and timing offset. This is further fulfilled by newly proposed estimation methods for channel parameters. Validated by extensive simulations, superior communication performance is attained by the proposed receiving scheme, tightly approaching the derived analytical bound.

As a future work, a holistic system parameter design will be carried out taking into account the performance of parameter estimation and data communication, as derived in Section V, and also the performance of radar sensing, as measured by, e.g., the range ambiguity function [14], [23]. As another future work, precoding at the radar will be designed to further improve communication performance in fading channels.

References

[1] X. You *et al.*, "Towards 6g wireless communication networks: Vision, enabling technologies, and new paradigm shifts," *SCIENCE CHINA Information Sciences*, pp. https://doi.org/10.1007/s11 432–020–2955–6.

[2] J. A. Zhang, X. Huang, Y. J. Guo, J. Yuan, and R. W. Heath, "Multibeam for joint communication and radar sensing using steerable analog antenna arrays," *IEEE Trans. Veh. Technol.*, vol. 68, no. 1, pp. 671–685, Jan 2019.

[3] M. L. Rahman, J. A. Zhang, K. Wu, X. Huang, Y. J. Guo, S. Chen, and J. Yuan, "Enabling joint communication and radio sensing in mobile networks–a survey," *arXiv preprint arXiv:2006.07559*, 2020.

[4] S. C. Surender and R. M. Narayanan, "UWB noise-OFDM netted radar: Physical layer design and analysis," *IEEE Trans. Aerosp. Electron. Syst.*, vol. 47, no. 2, pp. 1380–1400, 2011.

[5] P. Kumari, J. Choi, N. González-Prelcic, and R. W. Heath, "IEEE 802.11ad-based radar: An approach to joint vehicular communication-radar system," *IEEE Trans. Veh. Technol.*, vol. 67, no. 4, pp. 3012–3027, April 2018.

[6] G. R. Muns, K. V. Mishra, C. B. Guerra, Y. C. Eldar, and K. R. Chowdhury, "Beam alignment and tracking for autonomous vehicular communication using IEEE 802.11 ad-based radar," in *INFOCOM WKSHPS*. IEEE, 2019, pp. 535–540.

[7] P. Kumari, S. A. Vorobyov, and R. W. Heath, "Adaptive virtual waveform design for millimeter-wave joint communication-radar," *IEEE Trans. Signal Process.*, pp. 1–1, 2019.

[8] P. Barrenechea, F. Elferink, and J. Janssen, "FMCW radar with broadband communication capability," in *2007 European Radar Conf.* IEEE, 2007, pp. 130–133.

[9] M. Nowak, M. Wicks, Z. Zhang, and Z. Wu, "Co-designed radar-communication using linear frequency modulation waveform," *IEEE Aerosp. Electron. Syst. Mag*, vol. 31, no. 10, pp. 28–35, 2016.

[10] F. Liu, C. Masouros, A. P. Petropulu, H. Griffiths, and L. Hanzo, "Joint radar and communication design: Applications, state-of-the-art, and the road ahead," *IEEE Trans. Commun.*, vol. 68, no. 6, pp. 3834–3862, 2020.

[11] F. Liu, L. Zhou, C. Masouros, A. Li, W. Luo, and A. Petropulu, "Toward dual-functional radar-communication systems: Optimal waveform design," *IEEE Trans. Signal Process.*, vol. 66, no. 16, pp. 4264–4279, 2018.

[12] K. Wu, J. A. Zhang, X. Huang, and Y. J. Guo, "Frequency-hopping MIMO radar-based communications: An overview," *arXiv preprint*, 2020.

[13] A. Hassanien, M. G. Amin, E. Aboutanios, and B. Himed, "Dual-function radar communication systems: A solution to the spectrum congestion problem," *IEEE Signal Process. Mag.*, vol. 36, no. 5, pp. 115–126, Sep. 2019.

[14] I. P. Eedara, A. Hassanien, M. G. Amin, and B. D. Rigling, "Ambiguity function analysis for dual-function radar communications using PSK signaling," in *52nd Asilomar Conf. Signals, Syst., and Computers*, Oct 2018, pp. 900–904.

[15] I. P. Eedara, M. G. Amin, and A. Hassanien, "Analysis of communication symbol embedding in FH MIMO radar platforms," in *2019 IEEE Radar Conf. (RadarConf)*, April 2019, pp. 1–6.

[16] I. P. Eedara and M. G. Amin, "Dual function FH MIMO radar system with DPSK signal embedding," in *2019 27th European Signal Process. Conf. (EUSIPCO)*, Sep. 2019, pp. 1–5.

[17] I. P. Eedara, M. G. Amin, and A. Hassanien, "Controlling clutter modulation in frequency hopping MIMO dual-function radar communication systems," in *IEEE International Radar Conf. (RADAR)*, 2020, pp. 466–471.

[18] W. Baxter, E. Aboutanios, and A. Hassanien, "Dual-function MIMO radar-communications via frequency-hopping code selection," in *2018 52nd Asilomar Conf. on Signals, Syst., and Computers*, Oct 2018, pp. 1126–1130.

[19] K. Wu, Y. J. Guo, X. Huang, and R. W. Heath, "Accurate channel estimation for frequency-hopping dual-function radar communications," in *2020 IEEE International Conference on Communications Workshops (ICC Workshops)*, 2020, pp. 1–6.

[20] K. Wu, J. A. Zhang, X. Huang, Y. J. Guo, and R. W. Heath Jr, "Waveform design and accurate channel estimation for frequency-hopping MIMO radar-based communications," *arXiv preprint arXiv:2009.13745*, 2020.

[21] K. Wu, J. A. Zhang, X. Huang, and Y. J. Guo, "Integrating secure and high-speed communications into frequency hopping MIMO radar," *arXiv preprint arXiv:2009.13750*, 2020.

[22] I. P. Eedara and M. G. Amin, "Performance comparison of dual-function systems embedding phase-modulated signals in fh radar (conference presentation)," in *Signal Processing, Sensor/Information Fusion, and Target Recognition XXIX*, vol. 11423. International Society for Optics and Photonics, 2020, p. 114230U.

[23] C. Chen and P. P. Vaidyanathan, "MIMO radar ambiguity properties and optimization using frequency-hopping waveforms," *IEEE Trans. Signal Process.*, vol. 56, no. 12, pp. 5926–5936, Dec 2008.

[24] Y. Zhang, Ling Huang, and Jian Song, "Phased array radar based angular domain channel estimation scheme for integrated radar-communication system," in *MILCOM 2016 - 2016 IEEE Military Commun. Conf.*, 2016, pp. 906–911.

[25] L. Huang, Y. Zhang, Q. Li, and J. Song, "Phased array radar-based channel modeling and sparse channel estimation for an integrated radar and communication system," *IEEE Access*, vol. 5, pp. 15 468–15 477, 2017.

[26] A. Babaei, W. H. Tranter, and T. Bose, "A practical precoding approach for radar/communications spectrum sharing," in *8th International Conf. Cognitive Radio Oriented Wireless Netw.*, 2013, pp. 13–18.

[27] B. Li and A. P. Petropulu, "Joint transmit designs for coexistence of mimo wireless communications and sparse sensing radars in clutter," *IEEE Transactions on Aerospace and Electronic Systems*, vol. 53, no. 6, pp. 2846–2864, 2017.

[28] F. Liu, A. Garcia-Rodriguez, C. Masouros, and G. Geraci, "Interfering channel estimation in radar-cellular coexistence: How much information do we need?" *IEEE Transactions on Wireless Communications*, vol. 18, no. 9, pp. 4238–4253, 2019.

[29] M. L. Rahman, J. A. Zhang, X. Huang, Y. J. Guo, and R. W. Heath Jr, "Framework for a perceptive mobile network using joint communication and radar sensing," *IEEE Trans. Aerosp. Electron. Syst.*, vol. 56, no. 3, pp. 1926–1941, 2020.

[30] J. Li and P. Stoica, *MIMO radar signal processing*. John Wiley & Sons, 2008.

[31] M. Wang, F. Gao, S. Jin, and H. Lin, "An overview of enhanced massive MIMO with array signal processing techniques," *IEEE J. Sel. Topics Signal Process.*, vol. 13, no. 5, pp. 886–901, 2019.

[32] Y. S. Cho, J. Kim, W. Y. Yang, and C. G. Kang, *MIMO-OFDM wireless communications with MATLAB*. John Wiley & Sons, 2010.

[33] K. Wu, W. Ni, J. A. Zhang, R. P. Liu, and Y. J. Guo, "Refinement of optimal interpolation factor for DFT interpolated frequency estimator," *IEEE Commun. Lett.*, pp. 1–1, 2020.

[34] A. Serbes, "Fast and efficient sinusoidal frequency estimation by using the DFT coefficients," *IEEE Trans. Commun.*, vol. 67, no. 3, pp. 2333–2342, March 2019.

[35] M. K. Simon and M.-S. Alouini, *Digital communication over fading channels*. John Wiley & Sons, 2005, vol. 95.

[36] M. G. Shayesteh and A. Aghamohammadi, "On the error probability of linearly modulated signals on frequency-flat Ricean, Rayleigh, and AWGN channels," *IEEE Trans. Commun.*, vol. 43, no. 2/3/4, pp. 1454–1466, 1995.

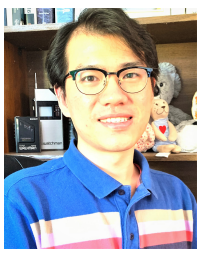

Kai Wu received the B.E. from Xidian University, Xi'an, China, in 2012, PhD from Xidian University in 2019, and PhD from the University of Technology Sydney (UTS), Sydney, Australia, in 2020. He is now a research fellow at the Global Big Data Technologies Centre, UTS. From Nov. 2017 to April 2018, he was a research assistant at the same centre. Before that, he was a visiting scholar at DATA61, CSIRO, Australia (Nov. 2016 - Nov. 2017). His research interests include array signal processing, and its applications in radar and communications.

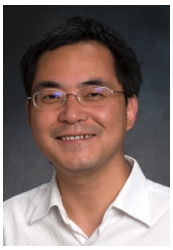

Dr J. Andrew Zhang (M'04-SM'11) received the B.Sc. degree from Xi'an JiaoTong University, China, in 1996, the M.Sc. degree from Nanjing University of Posts and Telecommunications, China, in 1999, and the Ph.D. degree from the Australian National University, in 2004.

Currently, Dr. Zhang is an Associate Professor in the School of Electrical and Data Engineering, University of Technology Sydney, Australia. He was a researcher with Data61, CSIRO, Australia from 2010 to 2016, the Networked Systems, NICTA, Australia from 2004 to 2010, and ZTE Corp., Nanjing, China from 1999 to 2001. Dr. Zhang's research interests are in the area of signal processing for wireless communications and sensing. He has published more than 200 papers in leading international Journals and conference proceedings, and has won 5 best paper awards. He is a recipient of CSIRO Chairman's Medal and the Australian Engineering Innovation Award in 2012 for exceptional research achievements in multi-gigabit wireless communications.

Xiaojing Huang (M'99-SM'11) received the B.Eng., M.Eng., and Ph.D. degrees in electronic engineering from Shanghai Jiao Tong University, Shanghai, China, in 1983, 1986, and 1989, respectively. He was a Principal Research Engineer with the Motorola Australian Research Center, Botany, NSW, Australia, from 1998 to 2003, and an Associate Professor with the University of Wollongong, Wollongong, NSW, Australia, from 2004 to 2008. He had been a Principal Research Scientist with the Commonwealth Scientific and Industrial Research Organisation (CSIRO), Sydney, NSW, Australia, and the Project Leader of the CSIRO Microwave and mm-Wave Backhaul projects since 2009. He is currently a Professor of Information and Communications Technology with the School of Electrical and Data Engineering and the Program Leader for Mobile Sensing and Communications with the Global Big Data Technologies Center, University of Technology Sydney (UTS), Sydney, NSW, Australia. His research interests include high-speed wireless communications, digital and analog signal processing, and synthetic aperture radar imaging. With over 32 years of combined industrial, academic, and scientific research experience, he has authored over 330 book chapters, refereed journal and conference papers, major commercial research reports, and filed 31 patents. Prof. Huang was a recipient of the CSIRO Chairman's Medal and the Australian Engineering Innovation Award in 2012 for exceptional research achievements in multigigabit wireless communications.

Y. Jay Guo (Fellow'2014) received a Bachelor Degree and a Master Degree from Xidian University in 1982 and 1984, respectively, and a PhD Degree from Xian Jiaotong University in 1987, all in China. His research interest includes antennas, mm-wave and THz communications and sensing systems as well as big data technologies. He has published four books and over 550 research papers including 300 journal papers, most of which are in IEEE Transactions, and he holds 26 patents. He is a Fellow of the Australian Academy of Engineering and Technology, a Fellow of IEEE and a Fellow of IET, and was a member of the College of Experts of Australian Research Council (ARC, 2016-2018). He has won a number of most prestigious Australian Engineering Excellence Awards (2007, 2012) and CSIRO Chairman's Medal (2007, 2012). He was named one of the most influential engineers in Australia in 2014 and 2015, respectively, and one of the top researchers in Australia in 2020.

Currently, he is a Distinguished Professor and the Director of Global Big Data Technologies Centre (GBDTC) at the University of Technology Sydney (UTS), Australia. Prior to this appointment in 2014, he served as a Director in CSIRO for over nine years. Before joining CSIRO, he held various senior technology leadership positions in Fujitsu, Siemens and NEC in the U.K.

Prof Guo has chaired numerous international conferences and served as guest editors for a number of IEEE publications. He is the Chair of International Steering Committee, International Symposium on Antennas and Propagation (ISAP). He was the International Advisory Committee Chair of IEEE VTC2017, General Chair of ISAP2022, ISAP2015, iWAT2014 and WPMC'2014, and TPC Chair of 2010 IEEE WCNC, and 2012 and 2007 IEEE ISCIT. He served as Guest Editor of special issues on "Low-Cost Wide-Angle Beam Scanning Antennas", "Antennas for Satellite Communications" and "Antennas and Propagation Aspects of 60-90GHz Wireless Communications," all in IEEE Transactions on Antennas and Propagation, Special Issue on "Communications Challenges and Dynamics for Unmanned Autonomous Vehicles," IEEE Journal on Selected Areas in Communications (JSAC), and Special Issue on "5G for Mission Critical Machine Communications", IEEE Network Magazine.

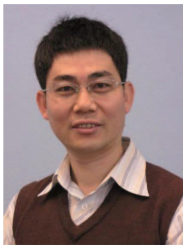

Jinhong Yuan (M'02–SM'11–F'16) received the B.E. and Ph.D. degrees in electronics engineering from the Beijing Institute of Technology, Beijing, China, in 1991 and 1997, respectively. From 1997 to 1999, he was a Research Fellow with the School of Electrical Engineering, University of Sydney, Sydney, Australia. In 2000, he joined the School of Electrical Engineering and Telecommunications, University of New South Wales, Sydney, Australia, where he is currently a Professor and Head of Telecommunication Group with the School. He has published two books, five book chapters, over 300 papers in telecommunications journals and conference proceedings, and 50 industrial reports. He is a co-inventor of one patent on MIMO systems and two patents on low-density-parity-check codes. He has co-authored four Best Paper Awards and one Best Poster Award, including the Best Paper Award from the IEEE International Conference on Communications, Kansas City, USA, in 2018, the Best Paper Award from IEEE Wireless Communications and Networking Conference, Cancun, Mexico, in 2011, and the Best Paper Award from the IEEE International Symposium on Wireless Communications Systems, Trondheim, Norway, in 2007. He is an IEEE Fellow and currently serving as an Associate Editor for the IEEE Transactions on Wireless Communications. He served as the IEEE NSW Chapter Chair of Joint Communications/Signal Processions/Ocean Engineering Chapter during 2011-2014 and served as an Associate Editor for the IEEE Transactions on Communications during 2012-2017. His current research interests include error control coding and information theory, communication theory, and wireless communications.